
Return-Aligned Decision Transformer

Tsunehiko Tanaka
Waseda University
tsunehiko@fuji.waseda.jp

Kenshi Abe
CyberAgent
abekenshi1224@gmail.com

Kaito Ariu
CyberAgent
kaitoariu@gmail.com

Tetusro Morimura
CyberAgent
morimura_tetsuro@cyberagent.co.jp

Edgar Simo-Serra
Waseda University
ess@waseda.jp

Abstract

Traditional approaches in offline reinforcement learning aim to learn the optimal policy that maximizes the cumulative reward, also known as return. However, as applications broaden, it becomes increasingly crucial to train agents that not only maximize the returns, but align the actual return with a specified target return, giving control over the agent’s performance. Decision Transformer (DT) optimizes a policy that generates actions conditioned on the target return through supervised learning and is equipped with a mechanism to control the agent using the target return. However, the action generation is hardly influenced by the target return because DT’s self-attention allocates scarce attention scores to the return tokens. In this paper, we propose Return-Aligned Decision Transformer (RADT), designed to effectively align the actual return with the target return. RADT utilizes features extracted by paying attention solely to the return, enabling the action generation to consistently depend on the target return. Extensive experiments show that RADT reduces the discrepancies between the actual return and the target return of DT-based methods.

1 Introduction

Offline reinforcement learning (RL) focuses on learning optimal policies using trajectories from offline datasets [1–5]. Many methods in offline RL traditionally aim to learn the optimal policy that maximizes the cumulative reward, also known as return. On the other hand, aligning cumulative rewards with a given target value is beneficial and required in many RL applications. For example, in video game development [6], developers seek AI opponents that can adjust performance to match beginners, amateurs, and masters. The AI opponents should adjust their performance to the levels intended by the developers. In attempts to replace human testers with RL agents in game playtesting [7–10], accurate

performance control contributes to improving the evaluation of feedback from the testing. Such agents are also needed in the development of educational tools [11] and traffic simulations [12–14]. We refer to the performance intended by the developers as the *target return*, and the cumulative reward obtained by the agent as the *actual return*. Despite the importance explained so far, existing

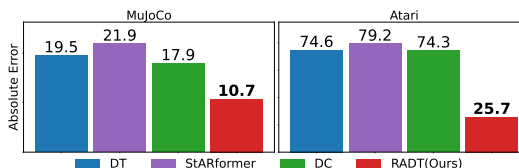


Figure 1: **Absolute errors between the target return and the actual return in both the MuJoCo and Atari domains.** The discrepancies are normalized by the return range between the top 5% and bottom 95% within the dataset. RADT significantly reduces the discrepancies in both domains.

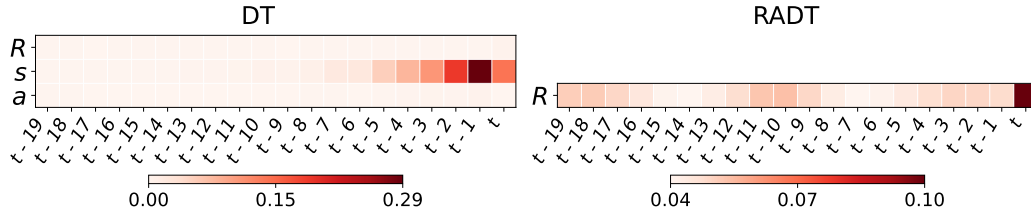


Figure 2: **Comparison of attention scores between DT and our RADT.** DT (left) does not assign much of attention scores to returns, suggesting that the features underlying action generation may not contain significant information about returns. Since the total attention scores sum up to one, the allocation to returns decreases if a large portion of attention is allocated to states and actions. In contrast, RADT (right) assigns attention scores only to returns, thus generating actions depending on the target return. A more detailed analysis is provided in Sec. 3.

approaches exhibit discrepancies between the actual return and target return, as shown in Fig. 1, which significantly lower the quality of the agents. By enabling the agent to align the actual return with the target return, for example, AI opponents can adjust their performance to the user’s skill levels, which contributes to game design with an excellent user experience. Furthermore, this capability enables the agent to accurately mimic a wide range of user behaviors, allowing for more precise evaluations during playtesting and simulations. This is expected to contribute to the development of superior games, educational tools, plans to alleviate traffic congestion, etc. In this work, we aim to align the actual return with the target return, enabling control of the agent’s performance based on the target return.

Decision Transformer (DT) [15] optimizes a policy that generates actions conditioned on the target return through supervised learning, and is equipped with a mechanism to control the agent using the target return. Specifically, this model takes a sequence comprising future desired returns, past states, and actions as inputs, and outputs actions using a transformer architecture [16]. In the self-attention mechanism of the transformer, each token incorporates significant features of the input sequence based on the relative importance of all tokens, also known as the attention score. DT uses the self-attention mechanism to condition the generation of actions, disseminating return information throughout the input sequence. However, DT struggles to match the actual return with the target return. Figure 1 illustrates the absolute error between the target return and the actual return, showing that the error of DT is significant. Our analysis reveals that DT’s self-attention allocates scarce attention scores to the returns within the input sequence, as shown in Fig. 2. This suggests that the return information almost disappears after passing through the DT’s self-attention, leading DT to generate actions independently from the target return.

In this paper, we propose an architectural design to align the actual return with the target return. To focus on returns in action generation, we split the input sequence into return and state-action sequences, and uniquely handle the return sequence in our architecture. We consider two strategies for handling the return sequence. One strategy is to model all returns in the return sequence at once, while the other is to independently model each return in the return sequence. We introduce a novel architecture to realize these two strategies, *Return-Aligned Decision Transformer* (RADT). In our experiments, RADT shows a significant reduction in the absolute error between the actual return and the target return, decreasing it to 54.9% of DT’s error in the MuJoCo [17] domain and 34.4% in the Atari [18] domain. We evaluate our two strategies through an ablation study, demonstrating that each strategy is effective and can complement each other. Our contributions are summarized as follows: (a) We propose the Return-Aligned Decision Transformer (RADT), a new offline RL approach designed to align the actual return with the target return. (b) RADT splits the input sequence into return and state-action sequences, and uniquely handles the return sequence to reflect returns in action generation. (c) Our experiments demonstrate that RADT surpasses existing offline RL approaches in aligning.

2 Preliminary

We assume a finite horizon Markov Decision Process (MDP) with horizon T as our environment, which can be described as $\mathcal{M} = \langle \mathcal{S}, \mathcal{A}, \mu, P, R \rangle$, where \mathcal{S} represents the state space; \mathcal{A} represents

the action space; $\mu \in \Delta(\mathcal{S})$ represents the initial state distribution; $P : \mathcal{S} \times \mathcal{A} \rightarrow \Delta(\mathcal{S})$ represents the transition probability distribution; and $R : \mathcal{S} \times \mathcal{A} \rightarrow \mathbb{R}$ represents the reward function. The environment begins from an initial state s_1 sampled from a fixed distribution μ . At each timestep $t \in [T]$, an agent takes an action $a_t \in \mathcal{A}$ in response to the state $s_t \in \mathcal{S}$, transitioning to the next state $s_{t+1} \in \mathcal{S}$ with the probability distribution $P(\cdot | s_t, a_t)$. Concurrently, the agent receives a reward $r_t = R(s_t, a_t)$.

Decision Transformer (DT) [15] introduces the paradigm of transformers into the context of offline reinforcement learning. At each timestep t in the inference, DT takes a sequence of desired returns, past states, and actions as inputs, and outputs an action a_t . The input sequence of DT is represented as

$$\tau = (\hat{R}_1, s_1, a_1, \hat{R}_2, s_2, a_2, \dots, \hat{R}_t, s_t), \quad (1)$$

where \hat{R}_t represents the returns computed over the remaining steps¹. It is calculated as $\hat{R}_t = R^{\text{target}} - \sum_{t'=1}^{t-1} r_{t'}$. R^{target} is a given constant², which is the total desired return to be obtained in an episode of length T . We refer to R^{target} as a target return. Raw inputs, referred to as tokens, are individually projected into the embedding dimension by separate learnable linear layers for return, state, and action respectively, to generate token embeddings. Note that from this point onwards, we will denote tokens as \hat{R}_i, s_i, a_i . The tokens are processed using a Transformer-based GPT model [19]. The processed token s_t is input into the prediction head to predict the action a_t . The model is trained using either cross-entropy or mean-squared error loss, calculated between the predicted action and the ground truth from the offline datasets.

The transformer [16] is an architecture designed for processing sequential data, including the attention mechanism, residual connection, and layer normalization. The attention mechanism processes three distinct inputs: the query, the key, and the value. This process involves weighting the value by the normalized dot product of the query and the key. The weight is also known as the attention score, and is calculated as follows:

$$\alpha_{ij} = \text{softmax}(\langle q_i, k_{\ell=1}^n \rangle_j), \quad (2)$$

where $\alpha_{ij} = 0, \forall j > i$ denotes a causal mask and n denotes the input length. The causal mask prohibits attention to subsequent tokens, rendering tokens in future timesteps ineffective for action prediction. The i -th output token of the attention mechanism is calculated as follows:

$$z_i = \sum_{j=1}^n \alpha_{ij} \cdot v_j, \text{ where } \sum_{j=0}^n \alpha_{ij} = 1 \text{ and } \alpha_{ij} \geq 0. \quad (3)$$

DT uses self-attention, where query, key, and value are obtained by linearly different transformations of the input sequence,

$$q_i = \tau_i W^q, \quad k_i = \tau_i W^k, \quad v_i = \tau_i W^v, \quad (4)$$

Layer normalization standardizes the token features to stabilize learning. Residual connection avoids gradient vanishing by adding the input and output of attention layers or feed-forward layers. For further details on DT, refer to the original paper [15].

DT conditions action generation by employing the self-attention mechanism to disseminate return information throughout the input sequence. Despite its design, DT cannot align the actual return with the target return, as illustrated in Fig. 1. To address this challenge, our goal is to minimize the following absolute error between the target return R^{target} and the actual return $\sum_{t=1}^T r_t$ using a single model:

$$\mathbb{E} \left[\left| R^{\text{target}} - \sum_{t=1}^T r_t \right| \right]. \quad (5)$$

¹For practicality, only the last K timesteps are processed, rather than considering the full inputs.

² R^{target} is the total return of the trajectory in the dataset during training, and it is a given constant during inference.

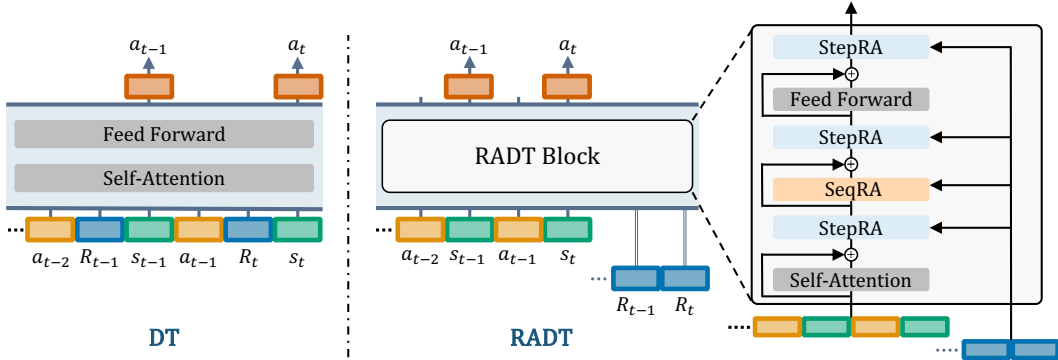


Figure 3: **Comparison between DT and the proposed RADT architecture.** RADT separates the return from the input sequence and applies two Return Aligners: Sequence Return Aligner (SeqRA) and Step-wise Return Aligner (StepRA).

3 Understanding Return Alignment Problems of DT

As shown in Fig. 1, DT struggles to align the actual return with the target return. In this section, we analyze the reasons behind DT’s difficulty in aligning. We hypothesize that the problem lies in the architectural design of DT. DT attempts to generate actions conditioned on the target return by including return tokens in the input sequence. Specifically, it aggregates tokens within the input sequence based on the attention scores in self-attention, as shown in Eq. (3). The objective is to incorporate the target return, which is embedded in the return tokens, into the features used in the prediction head. However, when the majority of the attention scores are allocated to state or action tokens, the allocation to return tokens decreases. This happens because the sum of the attention scores is one, based on Eq. (3). This reduction in allocation diminishes the information of the target return contained within the features used in the prediction head, potentially degrading the control performance of action generation by the target return.

To confirm our hypothesis, we analyze attention scores using DT model trained on the walker2d-medium dataset from MuJoCo, which has trajectories with diverse returns. Figure 2 (left) shows the episode averages of the attention scores for the first self-attention layer of DT. These scores represent the attention given to all tokens in the sequence against the state s_t token, which is used for predicting action a_t . We observe from Fig. 2 (left) that the attention scores are biased towards state tokens, with little allocation to return tokens. This observation suggests that the input sequence passing through self-attention is not absorbing much information about the target return. Given that DT applies the prediction head to this input sequence, it is expected that the target return would not significantly influence the predicted action.

4 Return-Aligned Decision Transformer

As previously discussed, DT struggles to align the actual return with the target return due to the under-allocation of attention scores to the return tokens. One intuitive way to solve this problem is to add a structure to extract features solely from the return tokens explicitly. To realize this intuition, we introduce *Return-Aligned Decision Transformer* (RADT).

We show the model structure of RADT in Fig. 3. We split the input sequence of τ in Eq. (1) into the return and other modalities: the return sequence τ_r and the state-action sequence τ_{sa}

$$\tau_r = (\hat{R}_1, \hat{R}_2, \dots, \hat{R}_t), \quad (6)$$

$$\tau_{sa} = (s_1, a_1, s_2, a_2, \dots, s_t). \quad (7)$$

For practical purposes, RADT processes only the last K timesteps of these sequences. We first apply self-attention to the state-action sequence τ_{sa} for credit assignment. We then process the state-action sequence τ_{sa} using our proposed method, ensuring τ_{sa} strongly depends on the return sequence τ_r . Finally, the action a_t is predicted from the s_t token of the processed state-action sequence τ_{sa} by the prediction head. The model is trained using the cross-entropy or mean-squared error loss between the predicted action and the ground truth.

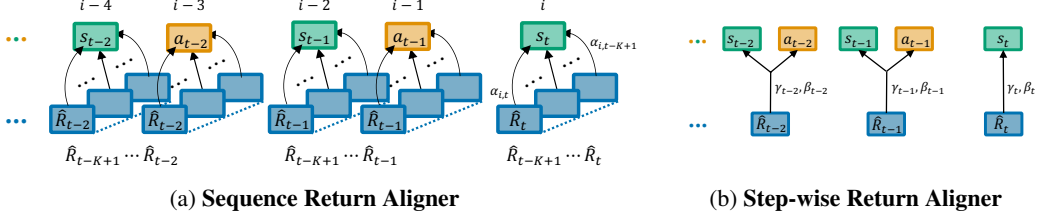


Figure 4: **Two strategies for extracting features from return sequence.** Both strategies receive the same state-action sequence τ_{sa} and return sequence τ_r . (a) SeqRA captures long-term dependencies from $(\hat{R}_{j-K+1}, \dots, \hat{R}_j)$. (b) StepRA focuses on a step-wise relationship from \hat{R}_j .

Two strategies can be considered for processing state-action sequences that depend on returns. The first strategy, *Sequence Return Aligner* (SeqRA), captures long-term dependencies within the return sequence, as shown in Fig. 4a. The second strategy, *Step-wise Return Aligner* (StepRA), focuses on a step-wise relationship, as illustrated in Fig. 4b. By implementing these strategies, RADT can focus on returns. This is illustrated by the attention scores from SeqRA, depicted in Fig. 2 (right). We will explain the details of SeqRA and StepRA in the following.

4.1 Sequence Return Aligner

SeqRA is designed to capture long-term dependencies within the return sequence τ_r , leveraging the effectiveness of sequence modeling introduced by DT in offline RL. We employ an attention mechanism to incorporate the return sequence τ_r into the state-action sequence τ_{sa} . We make the state-action sequence τ_{sa} as the query, and the return sequence τ_r as both the key and value.

$$q_i = \tau_{sa,i} W^q, \quad k_j = \tau_{r,j} W^k, \quad v_j = \tau_{r,j} W^v. \quad (8)$$

These query, key, and value are applied to Eq. (2) to get the attention scores. The attention score α_{ij} represents the relative importance of the return token $\tau_{r,j}$ in the return sequence for the token $\tau_{sa,i}$ in the state-action sequence. Note that we use a causal mask to ensure that tokens in the state-action sequence τ_{sa} cannot access future return tokens. We weight the return tokens based on the attention score, and obtain the token z_i in the state-action sequence that incorporates the return tokens from all timesteps as shown in Fig. 4a,

$$z_i = \sum_{j=0}^{K-1} \alpha_{it-j} \cdot \tau_{r,t-j} W^v, \quad \text{where} \quad \sum_{j=0}^{K-1} \alpha_{it-j} = 1 \quad \text{and} \quad \alpha_{it-j} \geq 0. \quad (9)$$

In many transformer-based models [16, 15, 20], residual connections that add the input and output queries of the attention mechanism are used to prevent gradient vanishing. Conversely, in SeqRA, we add two different types of sequences: τ_{sa} that does not contain any information of the return sequence and z that incorporates the return sequence. This addition potentially strengthens the influence of the state and action tokens on action generation by τ_{sa} , and decreases the impact of the return tokens on the output of this process. We therefore adaptively adjust the scale of z against τ_{sa} , following the powerful technique in computer vision for integrating two different types of features [21]. The process flow is shown in Fig. 5. We concatenate the multi-head attention input $\tau_{sa,i}$ and output z as a column vector $[z_i; \tau_{sa,i}] \in \mathbb{R}^{2D}$ and obtain dimension-wise scaling parameters λ

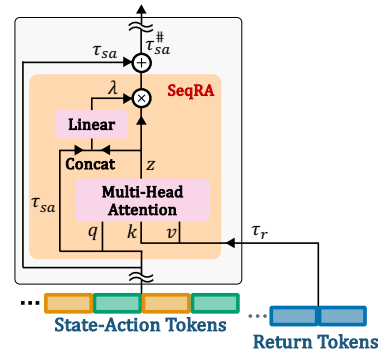


Figure 5: **Adaptive scaling for state-action sequence incorporating return sequence.** In the residual connection following the attention mechanism, τ_{sa} and z are added. Here, τ_{sa} does not hold return sequence information, while z incorporates the return sequence. We obtain the weighted sum $\tau_{sa}^{\#}$ using the scaling parameter λ , inferred from both τ_{sa} and z .

through a learnable affine projection. Using the scale λ , we define residual connection as

$$\lambda_i = W[z_i; \tau_{sa,i}] + b, \quad (10)$$

$$\tau_{sa,i}^\# = (1 + \lambda_i) \otimes z_i + \tau_{sa,i}, \quad (11)$$

where $W \in \mathbb{R}^{D \times 2D}$ and $b \in \mathbb{R}^D$ are learnable parameters, and \otimes denotes the Hadamard product. The output $\tau_{sa,i}^\#$ is used as the input sequence for the next layer. The choice of $1 + \lambda_i$ allows the model to start with a baseline scaling of one (simple addition) by zero-initialization of W and b , resulting in the scale of z_i and $\tau_{sa,i}$ being the same. This provides a stable starting point, from which the model can learn to adaptively adjust the scaling. As the training progresses, λ_i is updated to refine the balance between z_i and $\tau_{sa,i}$.

4.2 Step-wise Return Aligner

As shown in Eq. (9), the attention mechanism in SeqRA allocates the attention score, which sums up to one, to each return token. Consequently, depending on the assigned attention scores, the important return token for the current timestep may be excessively ignored. To address this issue, we introduce StepRA to ensure that each return token is not suppressed by others. StepRA independently incorporates each return token into the state or action token, as shown in Fig. 4b. It operates in parallel along the temporal axis.

In StepRA, the state and action tokens s_j, a_j are linearly transformed using the parameters $\gamma_j, \beta_j \in \mathbb{R}^D$ inferred from the return token r_j through MLPs. We apply the linear transformation after layer normalization for the state-action sequence to stabilize the training of the MLPs. Layer normalization ensures that the parameters of the MLPs act on data with the same range and distribution.

$$s_j^\# = (1 + \gamma_j) \otimes \text{LayerNorm}(s_j) + \beta_j, \quad (12)$$

$$a_j^\# = (1 + \gamma_j) \otimes \text{LayerNorm}(a_j) + \beta_j, \quad (13)$$

$$\gamma_j = \text{MLP}_\gamma(r_j), \beta_j = \text{MLP}_\beta(r_j), \quad (14)$$

where s_j represents the state token $\tau_{sa,2j-1}$, a_j represents the action token $\tau_{sa,2j}$, and r_j represents the return token $\tau_{r,j}$. The outputs $s_j^\#$ and $a_j^\#$ constitute the state-action sequence, which is used as the input sequence for the next layer. Similar to the $1 + \alpha_i$ in Eq. (11), by zero-initializing the parameters of the linear layer, Eqs. (12) and (13) can be considered the same as the standard layer normalization at the beginning of training. StepRA replaces DT’s layer normalization.

5 Experiments

In this section, we conduct extensive experiments to evaluate the performance of our RADT. First, we verify that RADT is effective in earning returns consistent with various given target returns, compared to other baselines. Next, we demonstrate through an ablation study that the two types of return aligners constituting RADT are effective individually, and using both types together further improves performance. Finally, we show that RADT is effective in maximizing the expected return.

5.1 Datasets

We evaluate RADT on continuous (MuJoCo [17]) and discrete (Atari [18]) control tasks in the same way as DT. MuJoCo requires fine-grained continuous control with dense rewards. We use four gym locomotion tasks from the widely-used D4RL [22] dataset: ant, hopper, halfcheetah, and walker2d. Atari requires long-term credit assignments to handle the delay between actions and their resulting rewards and involves high-dimensional visual observations. We use four tasks: Breakout, Pong, Qbert, and Seaquest. Similar to DT, we use 1% of all samples in the DQN-replay datasets as per Agarwal et al. [23] for training.

5.2 Baselines and settings

In order to evaluate our proposed model architecture, we utilize return-conditioned DT-based models with various architectural designs as baselines. Specifically, we use DT [15], StARformer [24], and

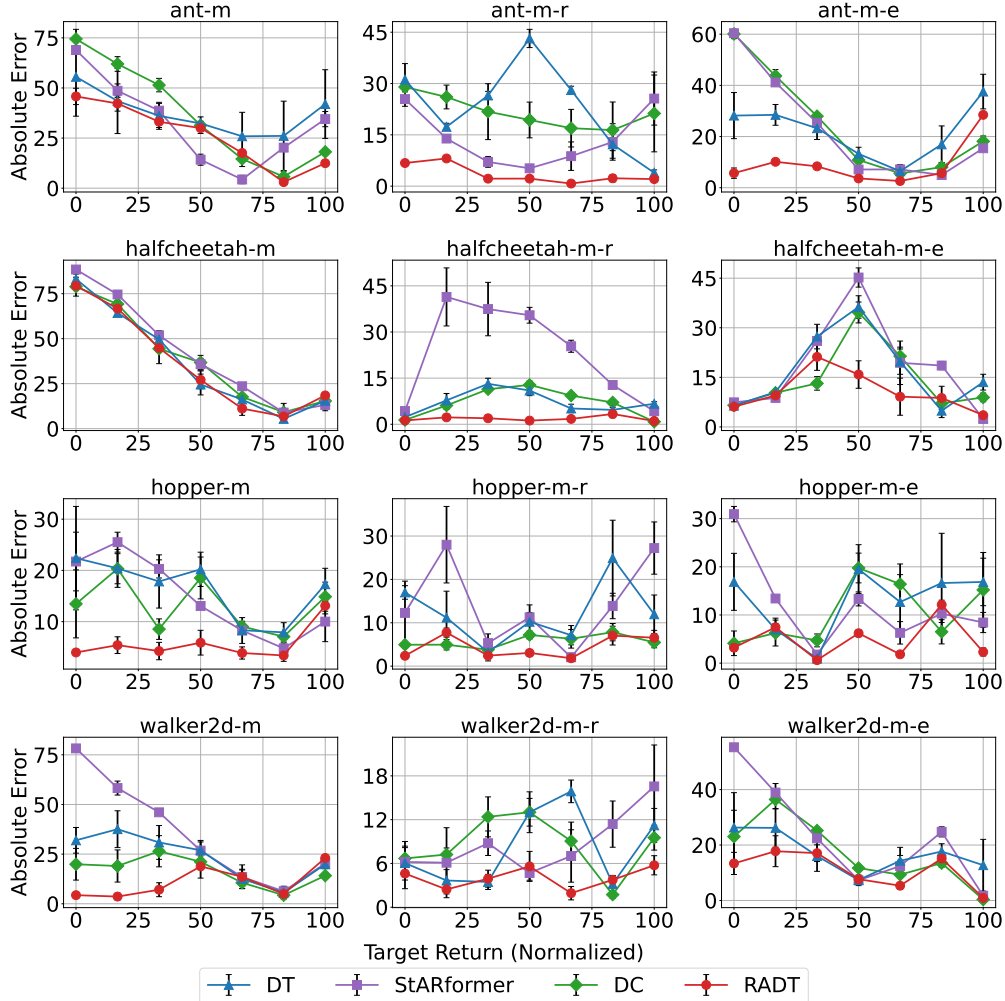


Figure 6: **Absolute error** comparison of RADT and baselines in MuJoCo domain. Each column represents a task. The x-axis is the target return. Target returns are divided into seven equally spaced points based on the cumulative reward of trajectories in the dataset, ranging from the bottom 5% to the top 5%. In this graph, the bottom 5% is represented as 0, and the top 5% as 100. The y-axis represents the absolute error between the actual return and the target return obtained from our simulations. We report the mean and standard error over three seeds. The dataset names are shortened: ‘medium’ to ‘m’, ‘medium-replay’ to ‘m-r’, and ‘medium-expert’ to ‘m-e’.

Decision ConvFormer (DC) [25]. We use the official PyTorch implementations for baselines. Please refer to Appendix C for the details of the baselines.

In MuJoCo, for each method, we train three instances with different seeds, and each instance runs 100 episodes for each target return. In Atari, for each method, we train three instances with different seeds, and each instance runs 10 episodes for each target return.

Target returns are set by first identifying the range of cumulative reward in trajectories in the training dataset, specifically from the bottom 5% to the top 5%. This identified range is then equally divided into seven intervals, not based on percentiles, but by simply dividing the range into seven equal parts. Each of these parts represents a target return. Further details are provided in Appendix D.

5.3 Results

The results are presented in Fig. 6 for the MuJoCo domain and Fig. 7 for the Atari domain. These figures plot the absolute error between the actual return and the target return, where lower is better.

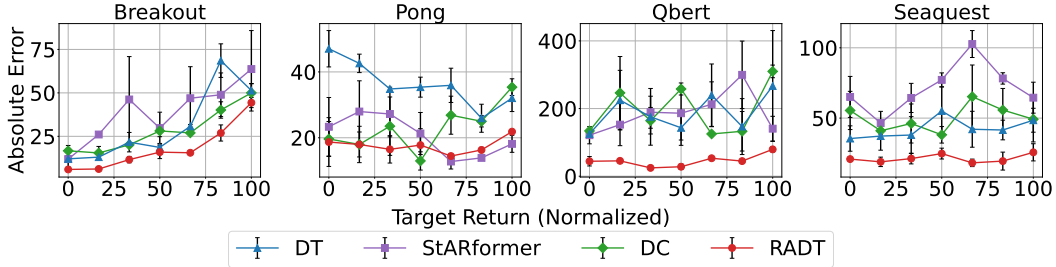


Figure 7: **Absolute error**↓ **comparison of RADT and baselines in the Atari domain.** The way to read these graphs is the same as in Fig. 6. We report the mean and standard error over three seeds.

Table 1: **Absolute error**↓ **comparison in the ablation study on SeqRA and StepRA.** We conduct the ablation study on the medium-replay dataset in MuJoCo. Each value indicates the sum of absolute errors across multiple target returns as defined in Sec. 5.2. We report the mean and standard error over three seeds, and normalize so that the average and variance of the DT’s results are 1.0 respectively.

Approach	SeqRA	StepRA	ant-m-r	halfcheetah-m-r	hopper-m-r	walker2d-m-r
DT			1.0±1.0	1.0±1.0	1.0±1.0	1.0±1.0
RADT w/o StepRA	✓		0.42±1.36	0.32±0.55	0.93±0.80	0.63±1.32
RADT w/o SeqRA		✓	0.19±0.29	0.28±0.49	0.59±0.62	0.56±0.59
RADT Full	✓	✓	0.15±0.28	0.25±0.42	0.36±0.24	0.50±0.74

The target returns are represented with the top 5% values as 100 and the bottom 5% values as 0. Detailed analysis using plots of the actual returns can be found in Appendix B.1.

MuJoCo domain. In the MuJoCo domain, as shown in Fig. 6, RADT outperforms other baselines in most target returns across all tasks. The baselines exhibit low sensitivity when the target return changes and they cannot consistently reduce the absolute error under a variety of target returns. In contrast, RADT consistently shows lower absolute errors across a wide range of target returns. These results suggest that RADT can effectively align the actual return with the target return in environments where fine-grained control is required with dense rewards.

Atari domain. Figure 7 shows that RADT surpasses the baselines in most target returns for all tasks in the Atari domain. We observe a tendency for the absolute errors of the baselines to be significant across most target returns. This suggests that the delay between actions and their resulting rewards makes accurate return modeling challenging in the Atari domain. Despite this challenge, RADT consistently exhibits smaller absolute errors across a wide range of target returns. These results suggest that RADT can effectively align the actual return with the target return in environments that require long-term credit assignments.

5.4 Ablation study

We conduct an ablation study for the two types of return aligners that constitute RADT on the medium-replay dataset in MuJoCo. The results are summarized in Tab. 1. Each value represents the sum of the absolute errors between the actual return and the target return across multiple target returns. These values are then normalized so that the average and standard error of the DT’s results are 1.0. Table 1 reports that introducing either SeqRA or StepRA individually proves to be effective. The combination of both aligners results in the smallest error across all tasks, implying that SeqRA and StepRA effectively complement each other. Please refer to Appendix. B.2 for the ablation study on the Atari domain.

5.5 Ability to maximize expected return

We conduct experiments on the MuJoCo and AntMaze domains to examine the ability to maximize the expected return, a standard task in offline RL. The MuJoCo domain features dense rewards, while the AntMaze domain features sparse rewards. We consider four baselines: CQL [26], DT [15],

Table 2: **Performance \uparrow comparison of return maximization in the MuJoCo domain.** We cite the results for DT, DC, and ODT from their reported scores. The results for CQL are cited from Kostrikov et al. [28]. We report the average across three seeds from our simulation results for RADT. The dataset names are shortened: ‘medium’ to ‘m’, ‘medium-replay’ to ‘m-r’, ‘medium-expert’ to ‘m-e’, ‘umaze’ to ‘u’, and ‘umaze-diverse’ to ‘u-d’. The boldface numbers denote the maximum score.

Method	CQL	DT	DC	ODT	RADT
halfcheetah-m	44.0	42.6	43.0	42.2	42.8 \pm 0.09
hopper-m	58.5	67.6	92.5	97.5	90.0 \pm 4.83
walker2d-m	72.5	74.0	79.2	76.8	75.6 \pm 0.57
halfcheetah-m-r	45.5	36.6	41.3	40.4	41.3 \pm 0.30
hopper-m-r	95.0	82.7	94.2	88.9	95.7 \pm 0.22
walker2d-m-r	77.2	66.6	76.6	76.9	75.9 \pm 1.55
halfcheetah-m-e	91.6	86.8	93.0	-	93.1 \pm 0.01
hopper-m-e	105.4	107.6	110.4	-	110.4 \pm 0.38
walker2d-m-e	108.8	108.1	109.6	-	109.7 \pm 0.16
antmaze-u	74.0	-	85.0	88.5	90.7 \pm 4.35
antmaze-u-d	84.0	-	78.5	56.0	80.7 \pm 2.37

DC [25], and ODT [27]. For RADT, we train three instances with different seeds, each running 100 episodes. We report the average of normalized returns in Tab. 2. The normalized returns are computed so that 100 represents the score of an expert policy, as per Fu et al. [22]. We can observe that RADT achieves competitive or superior results compared to the baselines. These results mean that the architectural design of RADT can not only align the actual return with the target return, but also excel in return maximization.

6 Related work

Return-conditioned offline RL Recent studies have focused on formulating offline reinforcement learning (RL) as a problem of predicting action sequences that are conditioned by goals and rewards [15, 29–33]. This approach differs from the popular value-based methods [26, 2, 28] by modeling the relationship between rewards and actions through supervised learning. Decision transformer (DT) [15] introduces the concept of desired future returns and improves performance by training the Transformer architecture [16] as a return-conditioned policy. Based on the DT framework, various advancements have been proposed for introducing value functions [34–36], finetuning models online [27], adjusting the length of the context [37], and improving the transformer architecture [24, 25].

Improving transformer architecture for offline RL Some efforts focus on refining the transformer architecture for offline RL. StARformer [24] introduces two transformer architectures, one aggregates information at each step, and the other aggregates information across the entire sequence. The image encoding process is improved by dividing the observation images into patches and feeding them into the transformer to enhance step information, similar to Vision Transformer [20]. Decision ConvFormer [25] replaces attention with convolution to capture the inherent local dependence pattern of MDP. While these architectures preserve the input sequence structure of the transformer, comprising returns, states, and actions, they do not directly tackle the challenge of diminishing the influence of returns on the decision-making process. In contrast, our research specifically aims to align the actual return with the target return.

7 Discussion

In this paper, we proposed RADT, a novel decision-making model for aligning the actual return with the target return in offline RL. RADT splits the input sequence into return and state-action sequences, and reflects returns in action generation by uniquely handling the return sequence. This unique handling includes two strategies that capture long-term dependencies and step-wise relationships

within the return sequence. Experimental results demonstrated that RADT has superior aligning capabilities compared to existing DT-based models. One limitation of our method is a slight increase in computational cost compared to DT. This could potentially be improved by introducing a lightweight attention mechanism, such as Flash Attention [38] into our SeqRA. We believe that the aligning capability of RADT can improve the usability of offline RL agents and expand their application range, which includes video game development, educational tool development, and traffic simulations.

References

- [1] Sergey Levine, Aviral Kumar, George Tucker, and Justin Fu. Offline reinforcement learning: Tutorial, review, and perspectives on open problems. *arXiv preprint arXiv:2005.01643*, 2020.
- [2] Scott Fujimoto and Shixiang Gu. A minimalist approach to offline reinforcement learning. In *Proc. of NeurIPS*, 2021.
- [3] Tianhe Yu, Aviral Kumar, Rafael Rafailov, Aravind Rajeswaran, Sergey Levine, and Chelsea Finn. Combo: Conservative offline model-based policy optimization. In *Proc. of NeurIPS*, 2021.
- [4] Ying Jin, Zhuoran Yang, and Zhaoran Wang. Is pessimism provably efficient for offline RL? In *Proc. of ICML*, 2021.
- [5] Haoran Xu, Li Jiang, Jianxiong Li, and Xianyuan Zhan. A policy-guided imitation approach for offline reinforcement learning. In *Proc. of NeurIPS*, 2022.
- [6] Georgios N. Yannakakis and Julian Togelius. *Artificial Intelligence and Games*. Springer, 2018.
- [7] Joakim Bergdahl, Camilo Gordillo, Konrad Tollmar, and Linus Gisslén. Augmenting automated game testing with deep reinforcement learning. In *Proc. of CoG*, 2020.
- [8] Sinan Ariyurek, Aysu Betin-Can, and Elif Surer. Automated video game testing using synthetic and humanlike agents. *IEEE Transactions on Games*, 2021.
- [9] Johannes Pfau, Antonios Liapis, Georgios N. Yannakakis, and Rainer Malaka. Dungeons & replicants ii: Automated game balancing across multiple difficulty dimensions via deep player behavior modeling. 2023.
- [10] Hyeon-Chang Jeon, In-Chang Baek, Cheong-mok Bae, Taehwa Park, Wonsang You, Taegwan Ha, Hoyoun Jung, Jinha Noh, Seungwon Oh, and Kyung-Joong Kim. Raidenv: Exploring new challenges in automated content balancing for boss raid games. 2023.
- [11] Adish Singla, Anna N Rafferty, Goran Radanovic, and Neil T Heffernan. Reinforcement learning for education: Opportunities and challenges. *arXiv preprint arXiv:2107.08828*, 2021.
- [12] Alexey Dosovitskiy, German Ros, Felipe Codevilla, Antonio Lopez, and Vladlen Koltun. CARLA: An open urban driving simulator. In *Proc. of CoRL*, 2017.
- [13] Eugene Vinitzky, Aboudy Kreidieh, Luc Le Flem, Nishant Kheterpal, Kathy Jang, Cathy Wu, Fangyu Wu, Richard Liaw, Eric Liang, and Alexandre M. Bayen. Benchmarks for reinforcement learning in mixed-autonomy traffic. In *Proc. of CoRL*, 2018.
- [14] Johannes Nguyen, Simon T. Powers, Neil Urquhart, Thomas Farrenkopf, and Michael Guckert. An overview of agent-based traffic simulators. *Transportation Research Interdisciplinary Perspectives*, 12:100486, 2021.
- [15] Lili Chen, Kevin Lu, Aravind Rajeswaran, Kimin Lee, Aditya Grover, Misha Laskin, Pieter Abbeel, Aravind Srinivas, and Igor Mordatch. Decision transformer: Reinforcement learning via sequence modeling. In *Proc. of NeurIPS*, 2021.
- [16] Ashish Vaswani, Noam Shazeer, Niki Parmar, Jakob Uszkoreit, Llion Jones, Aidan N Gomez, Lukasz Kaiser, and Illia Polosukhin. Attention is all you need. In *Proc. of NeurIPS*, 2017.
- [17] Emanuel Todorov, Tom Erez, and Yuval Tassa. MuJoCo: A physics engine for model-based control. In *Proc. of IROS*, 2012.
- [18] Marc G. Bellemare, Yavar Naddaf, Joel Veness, and Michael Bowling. The arcade learning environment: An evaluation platform for general agents. *Journal of Artificial Intelligence Research*, 47(1):253–279, 2013.
- [19] Alec Radford, Karthik Narasimhan, Tim Salimans, Ilya Sutskever, et al. Improving language understanding by generative pre-training. 2018.

- [20] Alexey Dosovitskiy, Lucas Beyer, Alexander Kolesnikov, Dirk Weissenborn, Xiaohua Zhai, Thomas Unterthiner, Mostafa Dehghani, Matthias Minderer, Georg Heigold, Sylvain Gelly, Jakob Uszkoreit, and Neil Houlsby. An image is worth 16x16 words: Transformers for image recognition at scale. In *Proc. of ICLR*, 2021.
- [21] Van-Quang Nguyen, Masanori Suganuma, and Takayuki Okatani. Grit: Faster and better image captioning transformer using dual visual features. In *Proc. of ECCV*, 2022.
- [22] Justin Fu, Aviral Kumar, Ofir Nachum, George Tucker, and Sergey Levine. D4rl: Datasets for deep data-driven reinforcement learning. *arXiv preprint arXiv:2004.07219*, 2020.
- [23] Rishabh Agarwal, Dale Schuurmans, and Mohammad Norouzi. An optimistic perspective on offline reinforcement learning. In *Proc. of ICML*, 2020.
- [24] Jinghuan Shang, Kumara Kahatapitiya, Xiang Li, and Michael S. Ryoo. StARformer: Transformer with state-action-reward representations for visual reinforcement learning. In *Proc. of ECCV*, 2022.
- [25] Jeonghye Kim, Suyoung Lee, Woojun Kim, and Youngchul Sung. Decision ConvFormer: Local filtering in MetaFormer is sufficient for decision making. In *Proc. of ICLR*, 2024.
- [26] Aviral Kumar, Aurick Zhou, George Tucker, and Sergey Levine. Conservative Q-learning for offline reinforcement learning. In *Proc. of NeurIPS*, 2020.
- [27] Qinqing Zheng, Amy Zhang, and Aditya Grover. Online decision transformer. In *Proc. of ICML*, 2022.
- [28] Ilya Kostrikov, Ashvin Nair, and Sergey Levine. Offline reinforcement learning with implicit Q-learning. In *Proc. of ICLR*, 2022.
- [29] Michael Janner, Qiyang Li, and Sergey Levine. Offline reinforcement learning as one big sequence modeling problem. In *Proc. of NeurIPS*, 2021.
- [30] Scott Emmons, Benjamin Eysenbach, Ilya Kostrikov, and Sergey Levine. Rvs: What is essential for offline RL via supervised learning? In *Proc. of ICLR*, 2022.
- [31] Shmuel Bar David, Itamar Zimmerman, Eliya Nachmani, and Lior Wolf. Decision S4: Efficient sequence-based RL via state spaces layers. In *Proc. of ICLR*, 2023.
- [32] Juergen Schmidhuber. Reinforcement learning upside down: Don't predict rewards—just map them to actions. *arXiv preprint arXiv:1912.02875*, 2019.
- [33] Rupesh Kumar Srivastava, Pranav Shyam, Filipe Mutz, Wojciech Jaśkowski, and Jürgen Schmidhuber. Training agents using upside-down reinforcement learning. *arXiv preprint arXiv:1912.02877*, 2019.
- [34] Taku Yamagata, Ahmed Khalil, and Raul Santos-Rodriguez. Q-learning decision transformer: Leveraging dynamic programming for conditional sequence modelling in offline RL. In *Proc. of ICML*, 2023.
- [35] Chenxiao Gao, Chenyang Wu, Mingjun Cao, Rui Kong, Zongzhang Zhang, and Yang Yu. Act: Empowering decision transformer with dynamic programming via advantage conditioning. *arXiv preprint arXiv:2309.05915*, 2023.
- [36] Hao Liu and Pieter Abbeel. Emergent agentic transformer from chain of hindsight experience. In *Proc. of ICML*, 2023.
- [37] Yueh-Hua Wu, Xiaolong Wang, and Masashi Hamaya. Elastic decision transformer. In *Proc. of NeurIPS*, 2023.
- [38] Tri Dao, Dan Fu, Stefano Ermon, Atri Rudra, and Christopher Ré. Flashattention: Fast and memory-efficient exact attention with io-awareness. In *Proc. of NeurIPS*, 2022.

A Broader impact

RADT can bring about a positive social impact by enabling adaptation to new application fields such as game production, educational content production, and simulations, as it can control the performance of agents more accurately. However, this advantage also comes with potential negative impacts such as the tracing of user behavior patterns. Such impact can be mitigated by applying methods such as blinding personal information during data generation and collection process.

B Additional experimental results

B.1 Further visualizations of main results

We show the comparisons of actual returns in Fig. 8 for the MuJoCo domain (corresponding to Fig. 6), and in Fig. 9 for the Atari domain (corresponding to Fig. 7). The black dotted line represents $y = x$, indicating that the actual return matches the target return perfectly. The closer to the black dotted line, the better the result.

MuJoCo domain. In all tasks except halfcheetah-medium, RADT is closer to the target return than the baseline is. It can be seen that ant-medium and halfcheetah-medium are struggling due to the extremely biased distribution of target returns in the datasets. In some tasks, the baselines show a constant actual return regardless of the input target return (e.g., DT in ant-medium-replay, StARformer in walker2d, DC and StARformer in ant-medium-expert, etc.). We believe this is due to the models overfitting the target return in areas where the data is concentrated.

Atari domain. We can see that the results of RADT are closer to the target returns than those of the baselines in all tasks from Fig. 9. In Qbert and Seaquest, the baselines achieve larger actual returns than the target returns. In contrast, RADT consistently achieves the actual return closest to the target return. In Breakout and Pong, StARformer achieves higher actual returns than other methods. We attribute this to the powerful vision encoder that StARformer equips based on the Vision Transformer [20]. Since the observations in the Atari domain are in image format, improving the vision encoder is advantageous. However, as evident from the results in Breakout, StARformer is excessively increasing the actual return beyond the target return. These results suggest that RADT has an advantage in aligning returns.

B.2 Additional ablation study

We conduct an ablation study for SeqRA and StepRA in the Atari domain. The experimental setup is the same as in Sec. 5.4. The results are summarized in Tab. 3. These results indicate that introducing either SeqRA or StepRA independently is effective. Furthermore, combining both aligners results in the minimum absolute error, implying a complementary relationship between SeqRA and StepRA. RADT w/o StepRA has the same or superior performance compared to RADT w/o SeqRA. This suggests that SeqRA is advantageous for the long-term credit assignments required in the Atari domain.

Table 3: **Absolute error** comparison in the ablation study on SeqRA and StepRA in the Atari domain. Each value indicates the sum of absolute error between the actual return and the target return, relative to the target returns in the main results. We report the mean and standard error over three seeds, and normalize such that the average and variance of the DT’s results are 1.0 respectively.

Approach	SeqRA	StepRA	Breakout	Pong	Qbert	Seaquest
DT			1.0±1.0	1.0±1.0	1.0±1.0	1.0±1.0
RADT w/o StepRA	✓		0.57±0.70	0.59±1.30	0.24±0.79	0.92±1.43
RADT w/o SeqRA		✓	0.61±0.66	0.91±1.70	0.24±0.12	0.95±1.14
RADT Full	✓	✓	0.55±0.74	0.51±0.59	0.22±0.09	0.49±0.35

C Baseline details

We use the model code for DT, StARformer, and DC from the following sources. DT: <https://github.com/kzl/decision-transformer>. StARformer: <https://github.com/elicassion/StARformer>. DC: <https://openreview.net/forum?id=af2c8EaKl8>. Although StARformer uses step-by-step rewards instead of returns, in our experiments, we employ return-conditioning using returns. This modification allows StARformer to condition action generation on target return. The original paper [24] states that this modification has a minimal impact on performance. For visual observations in the Atari domain, RADT and DC use the same CNN encoder as DT. StARformer, in addition to the CNN encoder, also incorporates more powerful patch-based embeddings like Vision Transformer [20].

The baseline results for aligning the actual return with the target return (Sec. 5.3) and the ablation study (Sec. 5.4) are from our simulations. The hyperparameters for each method in our simulations are set according to the defaults specified in their original papers or open-source codebases. The baseline results for maximizing the expected return (Sec. 5.5) stem from the original papers or third-party reproductions.

D Experimental details

D.1 Comparison of discrepancies

The discrepancies in Fig. 1 are calculated as the sum of the absolute errors between the actual return and target return across multiple tasks. The absolute error is normalized by the difference between the top 5% and bottom 95% of returns within the dataset.

D.2 Comparison of computational cost

Table 4 shows a comparison of the computational costs of DT and RADT. We compare the training time and GPU memory usage incurred when running 10^4 iterations of training on the hopper-medium dataset. In this comparison, we use an NVIDIA A100 GPU. RADT has slight increases in computation time and memory usage from DT. We believe these increases are due to the addition of SeqRA and StepRA. The computational costs of RADT could potentially be improved by introducing efficient attention mechanisms such as Flash Attention [38].

Table 4: Comparison of computational cost.

Method	Training Time (s)	GPU memory usage (GiB)
DT	450	0.030
RADT	562	0.034

D.3 Hyperparameters

The full list of hyperparameters of RADT can be found in Tab. 5 and Tab. 6. The hyperparameter settings of RADT are the same in both aligning and maximizing. The target returns used in maximizing are summarized in Tab. 7. The target returns used in aligning are automatically calculated from the dataset. For details, please refer to Sec. 5.2.

Table 5: **Hyperparameters settings of RADT in the MuJoCo domain and the AntMaze domain.** The dataset names are shortened: ‘medium’ to ‘m’, ‘medium-expert’ to ‘m-e’, ‘umaze’ to ‘u’, and ‘umaze-diverse’ to ‘u-d’.

Hyperparameter	Value
Number of layers	3
Number of attention heads	1
Embedding dimension	256, ant-m-e, halfcheetah-m, antmaze-u, antmaze-u-d 128, otherwise
Batch size	256, antmaze-u, antmaze-u-d 64, otherwise
Nonlinearity function	GELU, transformer SiLU, adaptive layer normalization
Context length K	20
Dropout	0.1
Learning rate	10^{-4}
Grad norm clip	0.25
Weight decay	10^{-4}
Learning rate decay	Linear warmup for first 10^5 training steps
Position Encoding	Sinusoidal Position Encoding

Table 6: **Hyperparameters settings of RADT in the Atari domain.**

Hyperparameter	Value
Number of layers	6
Number of attention heads	8
Embedding dimension	128
Batch size	512 Pong 128 Breakout, Qbert, Seaquest
Nonlinearity	ReLU encoder GELU transformer SiLU adaptive layer normalization
Encoder channels	32, 64, 64
Encoder filter size	$8 \times 8, 4 \times 4, 3 \times 3$
Encoder strides	4, 2, 1
Max epochs	5
Dropout	0.1
Learning rate	6×10^{-4}
Adam betas	(0.9, 0.95)
Grad norm clip	0.1
Weight decay	0.1
Learning rate decay	Linear warmup and cosine decay
Warmup tokens	$512 * 20$
Final tokens	$2 * 500000 * K$
Position Encoding	Sinusoidal Position Encoding

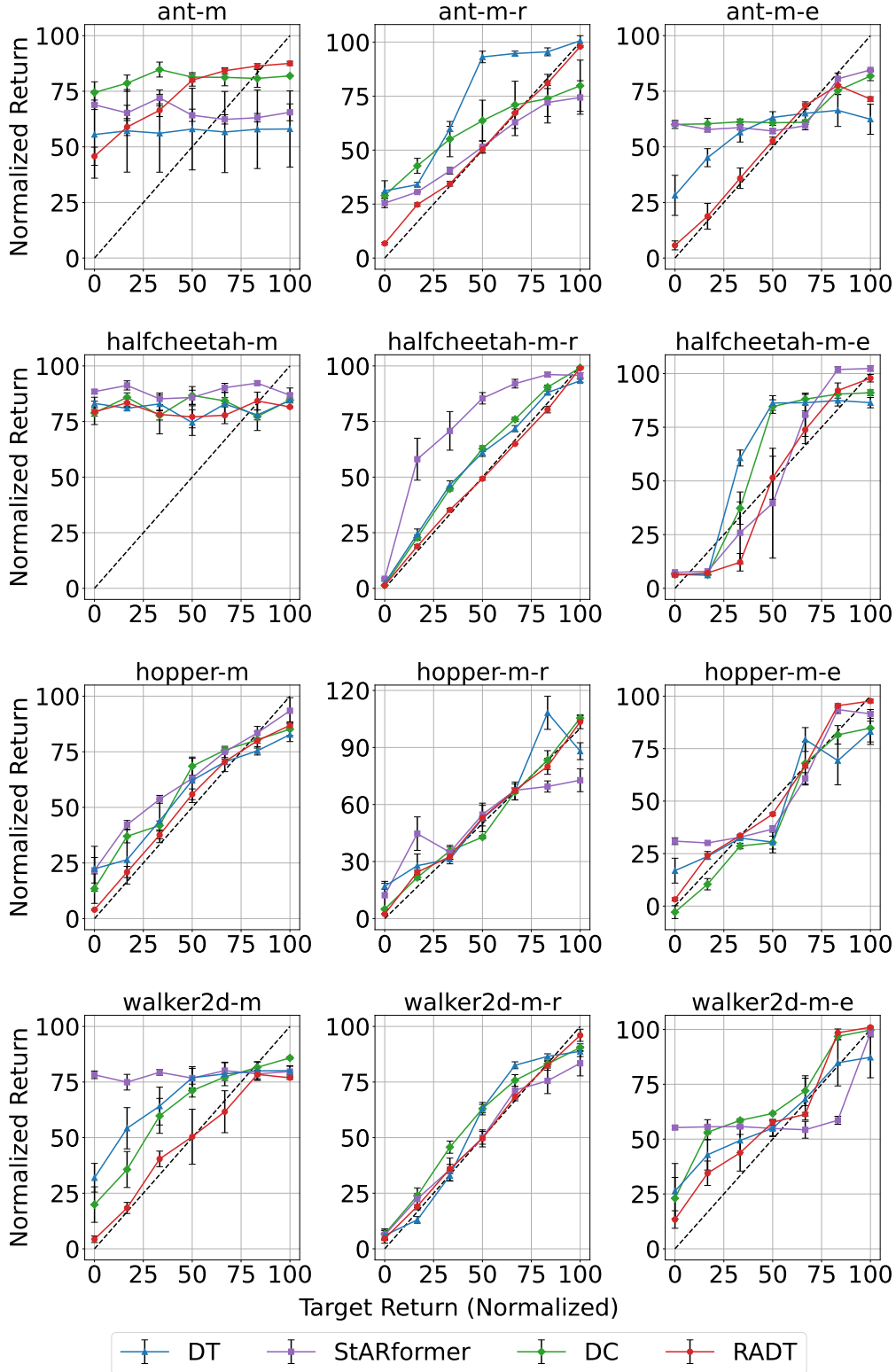


Figure 8: **Comparisons of actual returns per target return in the experiments of Fig. 6 for MuJoCo.** Each column represents a task. The x-axis represents the target return, and the y-axis represents the actual return. The x-axis and y-axis are normalized in the same way as in Fig. 6. Target returns are set in the same way as Fig. 6. The black dotted line represents $y = x$, indicating that the actual return matches the target return perfectly. We report the mean and standard error over three seeds. The dataset names are shortened: ‘medium’ to ‘m’, ‘medium-replay’ to ‘m-r’, and ‘medium-expert’ to ‘m-e’.

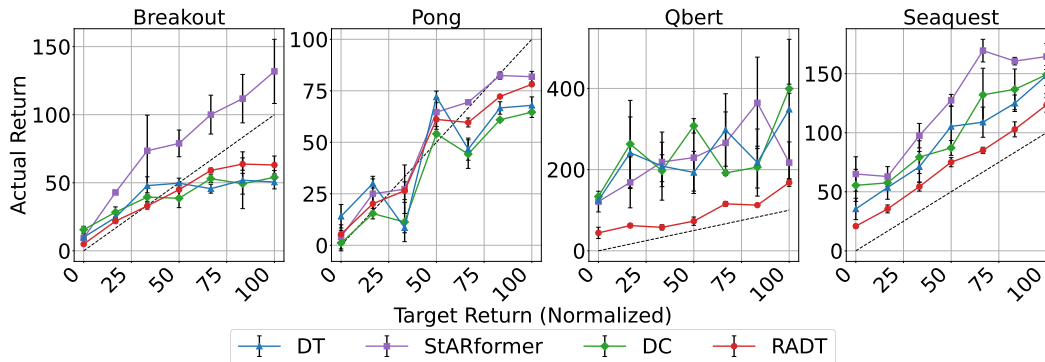


Figure 9: **Comparisons of actual returns per target return in the experiments of Fig. 7 for Atari.** Each column represents a task. The x-axis represents the target return, and the y-axis represents the actual return. The x-axis and y-axis are normalized in the same way as in Fig. 7. Target returns are set in the same way as Fig. 6. The black dotted line represents $y = x$, indicating that the actual return matches the target return perfectly. We report the mean and standard error over three seeds.

Table 7: **Target return inputs of RADT for maximizing expected return.**

Dataset	Target Return
halfcheetah-m	5100
hopper-m	6000
walker2d-m	3650
halfcheetah-m-r	5300
hopper-m-r	3200
walker2d-m-r	4500
halfcheetah-m-e	11400
hopper-m-e	3700
walker2d-m-e	6200
antmaze-u	4
antmaze-u-d	3